FIRST TECHNICAL PROGRESS REPORT

November, 1989

on

Predictive Models for Circulating Fluidized Bed Combustors

U.S. Department Energy Grant

DE-FG 22-89PC89769

D. Gidaspow, Principal Investigator

Department of Chemical Engineering

Illinois Institute of Technology

Chicago, Illinois 60616

ABSTRACT

The overall objective of this investigation is to develop experimentally verified models for circulating fluidized bed (CFB) combustors. The purpose of these models is to help American industry, such as Combustion Engineering, design and scale-up CFB combustors that are capable of burning U.S. Eastern high sulfur coals with low SO_x and NO_x emissions.

In this report, presented as a technical paper, solids distributions and velocities were computed for a PYROFLOW circulating fluidized bed system. To illustrate the capability of the computer code an example of coal-pyrite separation is included, which was done earlier for a State of Illinois project.

MULTIPHASE NAVIER-STOKES EQUATION SOLVER

by

D. Gidaspow, J. Ding and U. K. Jayaswal

Department of Chemical Engineering

Illinois Institute of Technology, Chicago, IL 60616

INTRODUCTION

A transient, two dimensional multiphase computer code for the solution of generalization of Navier Stokes equations for multiphase particulate flow was developed. The particulate viscosities are either an input into the code or are obtained from fluctuating energy equations derived from the Boltzman equation for velocity distribution of particles.

In this paper the computer code is applied to the solution of two engineering problems. The first problem deals with the predictions of solids circulation and hold-up in a commercial circulating fluidized bed boiler. The second problem deals with the design of an electrostatic separator which we propose to use in desulfurizing coal which is to be injected into a pulverized coal combustor. Although the partial differential equations that we are solving are well-posed as an initial value problem, in both situations discussed in this paper, a mathematical problem of how to prescribe boundary conditions for the particulate phases needs to be solved (Tsuo and Gidaspow, 1989). This problem is severe due to the backflow of solids. In the circulating fluidized bed problem, the system is taken to be closed for the solids by modeling the whole loop. This approach also gives us the high concentration of the solids in the bottom part of the riser which was not obtained when

an inlet velocity was prescribed (Tsuo and Gidaspow, 1989). In the electrostatic separator problem the backflow problem does not arise in a good design. In other cases the geometry was extended to provide a bag for collecting the particles. This approach of using a closed system or extending the geometry of the system with a variable mesh finite difference approximation has removed the issue of prescribing the proper boundary conditions.

A review of modeling of the hydrodynamics of fluidization of bubbling beds by D. Gidaspow (1986) showed that inviscid two-fluid models were able to predict a great deal of the behavior of bubbling beds because the dominant mechanism of energy dissipation is the drag between the particles and the fluid. The formation, the growth and the bursting of bubbles were predicted. Predicted wall-to-bed heat transfer coefficients and velocity profiles of jets agreed with measurements. Time average porosity distributions agreed with measurements done using gamma-ray densitometers without the use of any adjustable parameters. However, inviscid models could not correctly predict rates of erosion around tubes immersed into fluidized beds. To correctly model such behavior, granular stresses involving solids viscosity were added into the computer model. This viscosity arises due to random collision of particles. Several models for this viscosity were investigated and the results compared to measurements of solids distributions in two-dimensional beds and to particle velocities reported in the literature.

While in the case of bubbling beds the solids viscosity plays the role of a correction, modeling of a circulating fluidized bed (CFB) without a viscosity is not possible. Estimated solids viscosities were used in the two fluid hydrodynamic model, to predict radial solids distributions and solids velocities which matched the experimental distributions (Gidaspow, et al., 1989). Most important, the model

predicted cluster formation and transient internal circulation which is responsible for the favorable characteristics of CFBs, such as good wall-to-bed heat transfer. Video tape movies of computations compared favorably with high speed movies of the experiments.

In the dense phase regime of the CFB's, corresponding to volume fractions of about ten percent of solids, a core-annular type of flow regime, with solids descending down at the wall, was computed. (Tsuo and Gidaspow, 1989). The computed solids velocity profiles and radial solids concentrations agreed with measurements done at IGT (Bader, et al. 1988)

VISCOUS HYDRODYNAMIC MODELS

The physical principles used are the conservation laws of mass, momentum and energy for each phase, the fluid phase and the particulate phases. This approach is similar to that of Soo (1967) for multiphase flow and of Jackson (1985) for fluidization. A Newtonian type of constitutive equation for the surface stress of phase "k" is an appropriate first approximation, since the surface stress of phase "k" will depend at least on its symmetrical gradient of velocity. The emerging kinetic theory of granular flow provides a physical motivation for such an approach. Hence the general balance laws of mass and momentum for each phase, with phase change, are given by Equations (1) and (2) and the constitutive equation for the stress is given by Equation (3).

CONTINUITY EQUATION FOR PHASE k

$$\frac{\partial}{\partial t}(\epsilon_k \rho_k) + \nabla \cdot (\epsilon_k \rho_k \mathbf{v_k}) = \dot{m}_k \tag{1}$$

MOMENTUM EQUATION FOR PHASE k

$$\frac{\partial}{\partial t}(\epsilon_k \rho_k \mathbf{v_k}) + \nabla \cdot (\epsilon_k \rho_k \mathbf{v_k} \mathbf{v_k}) = \epsilon_k \rho_k \mathbf{g} + q_k \mathbf{E} + \nabla \cdot [\tau_\mathbf{k}] + \beta(\mathbf{v_l} - \mathbf{v_k}) + \dot{m}_k \mathbf{v_k} \quad (2)$$

acceleration of phase k = gravity+ electric+ stress+drag force+ phase change
force or particle-particle momentum
Interaction

CONSTITUTIVE EQUATION FOR PHASES

$$[\tau_\mathbf{k}] = [-p_k + \epsilon_k \xi_k \nabla \cdot \mathbf{v_k}][\mathbf{I}] + 2\epsilon_k \mu_k (\nabla^s \mathbf{v_k}) \quad (3)$$

These equations are similar to Bowen's (1976) balance laws for multicomponent mixtures. The principle difference is the appearance of the volume fraction of phase "k" detoned by ϵ_k. In the case of phases not all the space is occupied at the same time by all the phases, as it is by components. As in the case of the mixture equations for components, the mixture equations for phases show that the sum of the phase change productions in Equation (1) is zero and the sum of the drag forces in Equation (2) is zero. In convective form the phase change momentum in Equation (2) is zero, insuring invariance under a change of frame of reference for translation. Equation (3) is the usual Newtonian expression for the stress which arises from the assumption that the stress is a function of its own symmetrical gradient of velocity. For the fluid p_k is the fluid pressure. When this form is substituted into the momentum equation, the result is not the usual momentum balance presented by Gidaspow (1986) and widely used in gas-liquid two phase flow. It is a slightly modified version of the momentum balance, called model B by Bouillard et al. (1989a). This model is unconditionally well-posed. It does not require the presence of $p_k(\epsilon_k)$ for stability and well-posedness.

The corresponding particulate momentum equations with zero particulate viscosities are the trajectory equations for particulate flow. Bouillard, et al. (1989a) have shown that this set of equations produces essentially the same numerical answers for fluidization as did the earlier conditionally stable model which has the fluid pressure in the gas and in the solids phases. In this model the drag and the stress relations have to be altered to satisfy Archimedis' buoyancy principle, as illustrated by Bouillard, et al. (1989b) and Gidaspow, et al. (1989). In this model the characteristics are real and distinct for one dimensional transient flow. The problem is well-posed as an initial value problem (see Appendix A). For the particular phase, p_k consists of the static normal stress and the dynamic stress, called solids pressure, which arises due to the collision of the particles. Model A was used for computing the behavior of the circulating fluidized bed, while model B was used to compute the three phase electrostatic separator problem. The complete equations for model A are summarized in Table I.

The kinetic theory model was used for computation of bubbling bed behavior (Ding and Gidaspow, 1989). This model is based on the granular flow theories developed by Savage (1983, 1988) and Jenkins and Savage (1983). The expressions given in their papers have been interpreted as the dynamic solids pressure in Equation ($T1.5a$), as solids bulk viscosity and as shear viscosity, in Equations ($T1.5b$) and ($T1.5c$), respectively. These properties are in terms of the granular temperature T for which a conservation equation is written, given by Equation ($T1.6$). The gas-particulate drag coefficients given in Table I are for the model A reviewed by Gidaspow (1986). The kinetic theory model, whose development is in progress by J. Ding, provides a good physical interpretation of the meaning of the solids viscosity for the particular phase.

For the circulating fluidized bed presented in this paper, a turbulent viscosity for the gas phase was added into the model. This was necessary because in the dilute regime the solids viscosity computed from the kinetic theory was too low. For estimating the turbulent viscosity, a simple Subgrid scale (SGS) model is applied. This model was first used by Deardorff (1971) for channel flow and was successfully tested for single phase and two phase confined jets entering a pulverized coal combustor (Fan et al., 1985). The SGS model simulates the local Reynolds stresses which arise from the averaging process over finite-difference grid volumes by about the crudest of methods, that involving an eddy coefficient with magnitude limited in some way by the size of the averaging domain. This domain is considered to be the grid volume in a detailed numerical integration. Then, the eddy coefficient becomes a "subgrid scale" coefficient. In the simple SGS model, μ_t is expressed as,

$$\mu_t = \rho_g (c_t \triangle)^2 (2[\mathbf{S_g}] \cdot [\mathbf{S_g}])^{\frac{1}{2}} \tag{4}$$

where $c_t \simeq 0.1$ is a model constant, $\triangle$ is the characteristic length of difference mesh size, and

$$[\mathbf{S_g}] = \frac{1}{2}[\nabla \mathbf{v_g} + (\nabla \mathbf{v_g})^T] \tag{5}$$

NUMERICAL SCHEME

The full governing equations along with the constitutive equations are solved for p, U_g, V_g, ϵ_k, U_k and V_k, $(k = 1,..N)$ using the ICE method (Rivard and Torrey, 1977; Syamlal, 1985) with appropriate initial and boundary conditions. The computations are carried out using a mesh of finite-difference cells fixed in

two-dimensional space (Eulerian mesh). The scalar variables are located at the cell center and the vector variables at the cell boundaries.

The well-posedness of the partial differential equations is shown in Appendix A. The time step is chosen to satisfy the Courant stability criterion. The numerical stability of the equations can be obtained using the von Neumann stability analysis, as illustrated by Lyczkowski, et al. (1978) and Prosperetti (1982).

PART I. TWO-PHASE FLOW IN A FULL SCALE PYROFLOW CFB

A PYROFLOW circulating fluidized bed system built for Goodrich Co. in Henry, Illinois (Johnk and Wietske, 1989) is shown in Figure 1. Our kinetic theory model is used to simulate this CFB flow system. The governing equations are given in Table 1.

To simulate the real process of PYROFLOW CFB, a number of simplifications have to be made. The dimensions of the CFB are estimated from a man shown in the Pyroflow system (Johnk and Wietske, 1989) at the left bottom of Figure 2. The simplified geometry, dimensions and flow conditions of the PYROFLOW CFB are sketched in Figure 3. The bed is assumed to be isothermal and running at room temperature. The diameter and density of the solid particles are 150 μm and 1714 kg/cm^3, respectively. The terminal velocity of this particle is about 1.1 m/s. The top of the standpipe is covered by a screen to prevent the particles from leaving the system. The system is open to atmosphere. At the bottom of the standpipe, gas is fed in at a minimum fluidizing velocity of 2.5 cm/s. An air inlet velocity at the bottom of the riser is set to be V_{gin} = 2 to 5 m/s. Initially the system is static. The particles are packed in the riser and the standpipe with a

porosity $\epsilon = 0.42$ and a height $h_0 = 4.5$ m. Non-uniform finite difference grids are used in the computation. They are shown in Figure 3.

Figure 4 shows the computed solid flow and gas flow patterns as a function of time, for inlet air velocity of $V_{gin} = 200$ cm/s. Due to initial effects, solids in the standpipe are blown up at 1 second of real time. Solids begin to discharge from the standpipe to the riser at 2 seconds. It takes about 5 seconds for most particles to reach the top of the riser. Since the outlet of the riser is at the right side, the solids near the left wall of the riser move down to the bottom and are then carried up by the inlet gas from 6 to 8 seconds. We can see a downflow near the right wall of the riser. The radial profiles of time averaged axial gas and solid velocities at a height of 10 m in the riser are shown in Figure 5. The slip velocities are generally not large. In the lower part of the riser, there is downflow near the right wall, whereas, towards the top of the riser, the downflow shifts to the left wall. The asymmetric behavior is due to the asymmetric inlet and outlet locations. Figure 6 shows the radial profiles of solid volume fraction in the riser at heights of 5 m and 10 m. We see again the asymmetric distribution of particles in the radial direction. Pressures in the riser and in the standpipe decrease with increasing height. Figure 7 shows the radial profiles of solid mass flux at heights of 5 m and 10 m in the riser. The maximum solid mass flux is obtained near the center.

Figure 8 shows the solid discharge velocities from the standpipe to the riser as a function of time for inlet gas velocity $V_{gin} = 2$ m/s, 3 m/s and 5 m/s. The negative discharge velocity is due to initial effects. After 5 seconds, the discharge rates are of the order of 1 m/s, which is consistent with the measured data of solids discharge from hoppers (Gidaspow et al., 1986).

The inlet solid mass flux into the riser for $V_{gin} = 200$ cm/s is shown in Figure

9. After 7 seconds, the inlet mass flow rates are approximately equal to the outlet mass flow rates. In Figure 9 the dashed line shows the maximum flux obtained from a pressure balance derived by Gidaspow, et al. (1983).

The cross-sectional area averaged solid volume fractions and the net flux of the solid mass are shown in Figures 10 and 11. The figures show that the flows are close to fully developed between heights of 5 m and 12 m. The pressure distributions in the CFB for $V_{gin} = 500$ cm/s is shown in Figure 12. The high pressure regions are near the solids entry. Here the pressure rises due to the conversion of the kinetic energy of the solids discharged into the riser into a static head.

We see that the kinetic theory model is able to simulate fluidization in a real full-scale circulating fluidized bed. For modeling the combustion process in a CFB, reaction kinetics and energy equations will be added into the computer code.

PART II. DESIGN OF AN ELECTROSTATIC SEPARATOR

Dry electrostatic separation is a potentially efficient method of removing pyrites from coal. The overall objective of our investigation is to develop improved dry electrostatic separation methods of removing sulfur-bearing compounds from Illinois coal. Electrostatic separation is the selective sorting of solid species by means of utilizing forces acting on charged or polarized bodies in an electric field. When coal is pulverized for combustion, iron pyrites occur as distinct particles that can be removed by the application of an electric field (Inculet et al.,1982; Gidaspow et al., 1987). Separation is possible because the pyrites particles acquire charges different from the rest of coal. This surface charge can be acquired triboelectrically, by induction or by corona discarge. The electric charges on coal and pyrites differ in magnitude, which provide the driving forces for coal-pyrites separation under

the influence of an externally applied electric field. An electrostatic separator was developed and tested experimentally (see Figure 13). However, progress in the past has been hampered by a lack of quantitative analysis of the process. This simulation study is an effort to understand the hydrodynamics of separation of coal and pyrites. It has led to the design of an efficient electrostatic separator.

The separation system considered in this study consists of a gas and two distinct particulate phases. The two types of particles, coal and pyrite, contain different surface charges and differ in density. The input variables include the surface charge of the particles, which were measured and an estimated solids viscosity.

Surface Charge of particles

To model the electrostatic separator, we need to know the surface charge of the particles. The electric force acting on a particle in an electrostatic fields is the product of its charge and the strength of the applied electric field, i.e., $q_k E$. The average surface charge per particle was measured by inserting a metalic ball probe through the sides of an electrostatic pneumatic conveyor. Both coal and pyrites carry negative charges. It is interesting to compare the electrical force with the gravitational force acting on a pyrite particle in a free-fall electrostatic separator. The electrostatic force acting on a sphere of radius $a_p = 10\mu m$ with a uniform surface charge q_p is $F_e = q_p E$. The gravitational force is $F_g = (4/3)\pi {a_p}^3 \rho g$. At an electrical field strength of $E = 1000 V/cm$, the ratio $F_e/F_g = 22.7$ for pyrite particles and $F_e/F_g = 5.2$ for coal particles.

Electrostatic Separator Modeling

Two different geometries of the electrostatic separator were considered for simulation. The geometries and the dimensions used in the simulation are shown in

Figure 14. A two-dimensional configuration was taken. The electrostatic separator in case I differs from the experimental separator because it uses a coarser screen size for pyrites removal to save computation time. In case II, a different geometry was used for coal-pyrite simulation. The electrodes were 10 cm apart. The inlet to this unit was a 2 cm rectangular jet opening at one end. There were two outlets, one 2 cm rectangular jet opening for the clean coal stream and the other a perforated collector outlet for the pyrites rich stream with a jet opening at the end. The electrical and transport properties of coal and pyrite particles are given in Table II. The solids mixture consisted of particles with a 95.6 wt % coal and 4.4 wt % pyrites.

A particle loading of 0.2 kg of coal per kg of air was assumed. Initially, the entire separation unit was empty. At time zero, the solid-gas mixture entered the separating unit in the form of a jet at a constant velocity and at an inlet pressure of 1.05 atm. (20 " of water, gauge). Solid and gas phases entered the inlet of separating unit at the same constant velocity. The feed velocity was varied from 2.28 m/s to 5.1 m/s. The pressure drop inside the separating unit was taken to be 0.01 atm/m (approx. 4 " of water). Electric field strengths of 1000 V/cm or 1800 V/cm were applied across the electrode of the separating unit to achieve separation.

The equations were solved using the I.I.T. Encore computer. Simulations were carried out until a steady state operation was achieved. For the present simulation cases approximately 2 seconds of real time was required for a steady state operation.

Figures 15 and 16 show a comparison of case I and case II simulations for coal-pyrites separation at an electric field strength of 1800 V/cm. In case I, the

coal and pyrites particles separate, but the opening to collect the pyrites particles is very big. Thus coal particles are also collected. This results in a poor coal-pyrite separation. The computed pyrite separations and coal recoveries are close to those measured (Gidaspow, et al., 1987).

Figures 17 and 19 show the concentration distribution plots for coal and pyrites in the two separators. Here, the top electrode, which has a negative polarity is relatively free of liberated pyrites. The concentration of liberated pyrites in the clean coal stream exit is also low. A certain amount of coal goes out with the pyrite rich stream. The computed velocity vector plots for air, coal and pyrites are shown in Figures 18 and 20. The flow of pyrites is generally smooth and is towards the electrode which is positively charged. Air velocity vectors show the existence of wake formation in the dead regions close to the entrance. There air recirculation takes place. There is some back-mixing of the coal particles with the incoming feed at the upper part of the separator close to the entrance.

These simulations show that although the pyrites can be removed from coal almost completely, the coal recovery is poor, as obtained experimentally. Figures 15 and 18 suggest that to obtain a more complete coal recovery higher inlet air velocities must be used. To still keep the pyrite removal very high, the geometry of the separator must also be optimized. The pyrite removal ports must be located where the pyrite particle trajectory hits the electrode. Design of such an improved separator is in progress.

APPENDIX A

Characteristic Analysis

The characteristic directions for the propagation of the gas and the solids have been examined for the one-dimension inviscid case. In the non-conservative form, the continuity and the momentum equations for gas-solids flow are as follows,

$$\bar{\mathbf{A}}\begin{pmatrix} \frac{\partial \epsilon_g}{\partial t} \\ \frac{\partial p}{\partial t} \\ \frac{\partial V_g}{\partial t} \\ \frac{\partial V_s}{\partial t} \end{pmatrix} + \bar{\mathbf{B}}\begin{pmatrix} \frac{\partial \epsilon_g}{\partial x} \\ \frac{\partial p}{\partial x} \\ \frac{\partial V_g}{\partial x} \\ \frac{\partial V_s}{\partial x} \end{pmatrix} = \bar{\mathbf{C}} \tag{A.1}$$

where

$$\bar{\mathbf{A}} = \begin{pmatrix} \rho_g & \frac{\epsilon_g}{C^2} & 0 & 0 \\ -\rho_s & 0 & 0 & 0 \\ 0 & 0 & \epsilon_g \rho_g & 0 \\ 0 & 0 & 0 & \epsilon_s \rho_s \end{pmatrix} \tag{A.2}$$

and

$$\bar{\mathbf{B}} = \begin{pmatrix} \rho_g V_g & \frac{\epsilon_g V_g}{C^2} & \epsilon_g \rho_g & 0 \\ -\rho_s V_s & 0 & 0 & \epsilon_s \rho_s \\ 0 & 1 & \epsilon_g \rho_g V_g & 0 \\ -G & 0 & 0 & \epsilon_s \rho_s V_s \end{pmatrix} \tag{A.3}$$

and

$$\bar{\mathbf{C}} = \begin{pmatrix} 0 \\ 0 \\ f_{gs} + f_{gw} + \epsilon_g \rho_g g \\ f_{sg} + f_{sw} + \epsilon_s \rho_s g \end{pmatrix} \tag{A.4}$$

where $C = \sqrt{\left(\frac{\partial p}{\partial \rho_g}\right)_T}$

The characteristic determinant is

$$|\bar{\mathbf{B}} - \lambda \bar{\mathbf{A}}| = 0$$

which can be represented as,

$$\begin{vmatrix} \rho_g(V_g-\lambda) & \frac{\epsilon_g}{C^2}(V_g-\lambda) & \epsilon_g\rho_g & 0 \\ -\rho_s(V_s-\lambda) & 0 & 0 & \epsilon_s\rho_s \\ 0 & 1 & \epsilon_g\rho_g(V_g-\lambda) & 0 \\ -G & 0 & 0 & \epsilon_s\rho_s(V_s-\lambda) \end{vmatrix} = 0 \qquad (A.5)$$

The characteristic roots, λ_i of the above determinant are

$$\lambda_{1,2} = V_g \pm \sqrt{\frac{C^2}{\epsilon_g}} \qquad (A.6)$$

and

$$\lambda_{3,4} = V_s \pm \sqrt{\frac{G}{\rho_s}} \qquad (A.7)$$

Since $\frac{C^2}{\epsilon_g} > 0$, and $\frac{G}{\rho_s} > 0$, this equation set has real and distinct characteristics, the system is hyperbolic. The problem is well-posed as an initial-value problem (Lyczkowski, *et al.*, 1978).

The characteristic directions also determine where the boundary conditions must be prescribed for a well-posed problem. Equation (A.6) shows that information about the gas must be prescribed at the inlet and at the exit, since the characteristic directions are positive and negative due to the large value of C. Although the form for the solid, as shown by equation (A.7), is similar to that for the gas, the value of G/ρ_s is small. Its square root is of the order of 1 m/sec for dense flow, for a volume fraction of solid of about 0.6. It is very low for dilute flow. Hence normally the characteristic directions for the solid are both positive. For small values of G, the characteristics are nearly equal. The particles essentially move with their own velocity, with the wave effect negligible. Hence in a CFB where there is reverse flow, a boundary condition for the solid must be prescribed at the top of the pipe.

In a strict sense, this analysis is not applicable to viscous flow. However, it is known that the viscous terms are a correction, since the viscous dissipations,

both in the gas and the solid phases, are much smaller than the dissipation due to the drag between the particles and the gas. Hence an inviscid analysis provides a useful guide. The introduction of a bend at the top of the pipe provided us with a valid boundary condition for the solid in the downflow region, whenever it existed. The normal component of the solid velocity was zero. Such a situation corresponds to the experimental conditions and to the industrial practice. The disadvantage of this approach is that a two-dimensional slice of the pipe had to be studied, because axial symmetry could no longer be 'sed.

ACKNOWLEDGEMENT

Modeling of the PYROFLOW CFB was supported by the Department of Energy coal research university grant no DE-FG 22-89PC89769 "Predictive Models for Circulating Fluidized Bed Combustors"

DISCLAIMER

Table I. GOVERNING EQUATIONS FOR PARTICULATE MULTIPHASE FLOW

In the following equations, the tensor is represented as [ ].

1. CONTINUITY EQUATION FOR PHASE $k(= g, s)$

$$\frac{\partial}{\partial t}(\epsilon_k \rho_k) + \nabla \cdot (\epsilon_k \rho_k \mathbf{v_k}) = \dot{m}_k \qquad (T1.1)$$

2. MOMENTUM EQUATION FOR PHASE $k(= g, s)$

$$\frac{\partial}{\partial t}(\epsilon_k \rho_k \mathbf{v_k}) + \nabla \cdot (\epsilon_k \rho_k \mathbf{v_k v_k}) = \epsilon_k \rho_k \mathbf{g} + q_k \mathbf{E} + \nabla \cdot [\tau_k] + \beta_{kl}(\mathbf{v_l} - \mathbf{v_k}) + \dot{m}_k \mathbf{v_k} \qquad (T1.2)$$

3. CONSTITUTIVE EQUATION FOR STRESS

$$[\tau_k] = [-p_k + \epsilon_k \xi_k \nabla \cdot \mathbf{v_k}][\mathbf{I}] + 2\epsilon_k \mu_k [\mathbf{S_k}] \qquad (T1.3)$$

$$[\mathbf{S_k}] = \frac{1}{2}[\nabla \mathbf{v_k} + (\nabla \mathbf{v_k})^T] - \frac{1}{3} \nabla \cdot \mathbf{v_k}[\mathbf{I}] \qquad (T1.3a)$$

3A. Turbulent Model for Gas Phase

$$\mu_{ge} = \mu_t + \mu_g = \rho_g (c_t \triangle)^2 (2[\mathbf{S_g}] \cdot [\mathbf{S_g}])^{\frac{1}{2}} + \mu_g \qquad (T1.3b)$$

with $c_t = 0.1$

3B. Empirical Solids Viscosity and Stress Model

$$\xi_s = -\frac{2}{3}\mu_s \qquad (T1.4a)$$

$$\nabla p_s = G(\epsilon_s) \nabla \epsilon_s \qquad (T1.4b)$$

$$G(\epsilon_s) = 10^{8.76\epsilon_s - 0.27} \qquad dynes/cm^2 \qquad (T1.4c)$$

$$\mu_s = 5 \; poises, \qquad (example) \qquad (T1.4d)$$

3C. Kinetic Theory Model

solids phase pressure

$$p_s = \epsilon_s \rho_s [1 + 2(1 + e)\epsilon_s g_0] T \qquad (T1.5a)$$

solid phase bulk viscosity

$$\xi_s = \frac{4}{3}\epsilon_s \rho_s d_p g_0 (1 + e)(\frac{T}{\pi})^{\frac{1}{2}} \qquad (T1.5b)$$

solid phase shear viscosity

$$\mu_s = \frac{4}{5}\epsilon_s \rho_s d_p g_0 (1 + e)(\frac{T}{\pi})^{\frac{1}{2}} \qquad (T1.5c)$$

radial distribution function

$$g_0 = \frac{3}{5}[1 - (\frac{\epsilon_s}{\epsilon_{s,max}})^{\frac{1}{3}}]^{-1} \qquad (T1.5d)$$

3C.1 Fluctuating energy $\frac{3}{2}T$ $(= \frac{1}{2} < C^2 >)$ equation

$$\frac{3}{2}[\frac{\partial}{\partial t}(\epsilon_s \rho_s T) + \nabla \cdot (\epsilon_s \rho_s \mathbf{v_s} T)] = [\tau_s] : \nabla \mathbf{v_s} - \nabla \cdot \mathbf{q} - \gamma - 3\beta T \qquad (T1.6)$$

collisional energy dissipation γ

$$\gamma = 3(1-e^2)\epsilon_s^2 \rho_s g_0 T(\frac{4}{d_p}(\frac{T}{\pi})^{\frac{1}{2}} - \nabla \cdot \mathbf{v_s}) \qquad (T1.6a)$$

flux of fluctuating energy $\mathbf{q}$

$$\mathbf{q} = -\kappa \nabla T \qquad (T1.6b)$$

conductivity of the fluctuating energy

$$\kappa = 2\rho_s \epsilon_s^2 d_p (1+e) g_0 (\frac{T}{\pi})^{\frac{1}{2}} \qquad (T1.6c)$$

4. GAS-SOLID DRAG COEFFICIENTS
for $\epsilon_g < 0.8$, (based on Ergun equation)

$$\beta_{sg} = 150\frac{\epsilon_s^2 \mu_g}{\epsilon_g (d_p \phi_s)^2} + 1.75\frac{\rho_g \epsilon_s |\mathbf{v_g} - \mathbf{v_s}|}{\phi_s d_p} \qquad (T1.7a)$$

for $\epsilon_g > 0.8$, (based on empirical correlation)

$$\beta_{sg} = \frac{3}{4} C_d \frac{\epsilon_g \epsilon_s \rho_g |\mathbf{v_g} - \mathbf{v_s}|}{d_p} \epsilon_g^{-2.65} \qquad (T1.7b)$$

where,

$$C_d = \frac{24}{Re_s}[1 + 0.15(Re_s)^{0.687}], \quad for \quad Re_s < 1000 \qquad (T1.8a)$$

$$C_d = 0.44, \quad for \quad Re_s \geq 1000, \qquad (T1.8b)$$

$$Re_s = \frac{\epsilon_g \rho_g |\mathbf{v_g} - \mathbf{v_s}| d_p}{\mu_g} \qquad (T1.8c)$$

5. PARTICLE-PARTICLE DRAG COEFFICIENTS

$$\beta_{klk,l \neq g} = \frac{3}{2}\alpha(1+e)\frac{\rho_k \rho_l \epsilon_k \epsilon_l (d_k + d_l)^2}{\rho_k d_k^3 + \rho_l d_l^3} |\mathbf{v_k} - \mathbf{v_l}| \qquad (T1.9)$$

Table II. Electrical and Transport Properties of Coal and Pyrites

Particle Diameter	20 μm
Density of coal	1.27 g / cm^3
Electric Charge of coal	-5.1×10^{-4} coul / kg
Density of pyrites	4.8 g / cm^3
Electric Charge of pyrites	-2.22×10^{-3} coul / kg
Solid viscosity	5 poise
Air viscosity	1.8×10^{-4} poise
Air temperature	25 °C

NOTATION

Abbreviation	Term
C	fluctuating velocity of particle, sonic velocity
C_d	drag coefficient
d_s	particle diameter
$\mathbf{E}$	electric field strength
e	coefficient of restitution
f	friction coefficient
G	solid stress modulus
$\mathbf{g}$	gravity
g_0	radial distribution function
$[\mathbf{I}]$	unit tensor
m	rate of phase production per unit volume
p	pressure
$\mathbf{q}$	flux vector of fluctuating energy
q_k	surface charge of particle per unit mass
Re_s	Reynolds number of particles
$[\mathbf{S}]$	deformation rate tensor
$\frac{3}{2}T$	fluctuating energy
t	time
V	Velocity
$\mathbf{v}$	velociy vector
Greek letters	
α	parameters in Jenkins and Savage's model

β	drag coefficient between phases
γ	collisional energy dissipation
ϵ	volume fraction
$\epsilon_{s,max}$	maximum solid volume fraction
ζ	solids vorticity
κ	conductivity of fluctuating energy
λ	characteritic root
μ	shear viscosity
μ_{ge}	effective gas viscosity
ξ	bulk viscosity
ρ	density
τ	stress
ϕ_c	collisional rate of change
ϕ_s	particle sphericity
ψ	single-particle quantity

Subscripts

k, l	phase k or l
g	gas phase
s	solid phase
w	wall

Superscripts

c	collisional part
k	kinetic part
T	transpose

REFERENCES

Bader,R.J., Findlay, and Knowlton,T.D.(1988). Gas/Solid Flow Patterns in a 30.5-cm-Diameter Circulating Fluidized Bed. in *Circulating Fluidized Bed Technology II*, edited by P. Basu and J.F.Large, Pergamon Press, 123-137.

Bouillard,J.X., Lyczkowski,R.W., and Gidaspow,D. (1989a). Porosity Distributions in a Fluidized Bed with an Immersed Obstacle. *AIChE J.* **35**, no.6, 908-922.

Bouillard,J.X., Lyczkowski,R.W., Folga,S.,Gidaspow,D. and Berry,G.F.(1989b). Hydrodynamics of Erosion of Heat Exchanger Tubes in Fluidized Bed Combustors. *Canadian J. Chem. Eng.*, vol.67, 218-229.

Bowen,R.M.(1976). Theory of Mixtures, in *Continuum Physics*, editor A.C.Eringen, Vol. III, 1-117, Academic Press, New York.

Deardorff,J.W.(1971). On the Magnitude of the Subgrid Scale Eddy Coefficient. *J. Comput. Phys*, **7**, 120-133.

Ding,J., and Gidaspow, D.(1989). A Bubbling Fluidization Model Using Kinetic Theory of Granular Flow. Submitted to: *AIChE J.*

Fan,Z.Q.,Zhang,B.Z., and Ding,J.(1985). Prediction of Gas-Particle Two-Phase Flows in Combustion. *Int. Symp.-Workshop on Particulate and Multiphase Processes and 16th Annual Meeting of the Fine Particle Society.* Miami Beach, Florida, U.S.A., Proc., Hemisphere Publishing Co. 163-172.

Gidaspow,D., Tsuo,Y.P., and Ding J.(1989). Hydrodynamics of Circulating and Bubbling Fluidized Beds. *Material Issues in Circulating Fluidized-Bed Combustor Workshop*, Argonne National Laboratory, Argonne, Illinois, June 19-23.

Gidaspow,D., Gupta,R., Mukherjee,A. and Wasan,D.(1987). Separation of Pyrites from Illinois Coals using Electrofluized Beds and Electrostatic Sieve Conveyors. *Processing and Utilization of High Sulfur Coals II*, edited by Y.P.Chugh and R.D.Caudle, Elsevier, New York.

Gidaspow,D.(1986). Hydrodynamics of Fluidization and Heat Transfer: Supercomputer Modeling. *Appl. Mech. Rev.*, **39**, no.1, 1-23.

Gidaspow,D., Ding,J., and Luo,K.M. (1986). A Measurement of the Modulus of Elasticity Using Critical Flow Theory. *DOE Report*, DE86011993, Apr. 1986.

Gidaspow,D. and Ettehadieh,B. (1983). Fluidization in Two Dimentional Beds with a Jet. Part II. Hydrodynamic Modeling. *I&EC Fundam*, **22**, 193-201.

Inculet,I.I., Bergougnou,M.A., and Brown,J.D.(1982). Electrostatic Beneficiation of Coal, *Physical Cleaning of Coal*, edited by Y.A.Liu, Dekker, 87.

Jackson,R.(1985). Hydrodynamic Stability of Fluid-Particle Systems. in *Fluidization*, edited by J.F.Davidson, R. Clift and D. Harrison, Academic Press, 47-72.

Jenkins,J.T. and Savage,S.B.(1983). A Theory for the Rapid Flow of Identical,Smooth,Nearly Elastic,Spherical Particles. *J.Fluid Mech.*, **130**, 187-202.

Johnk,C., and Wietzke,D.(1989). Ahlstrom PYROFLOW Circulating Fluidized Bed Boiler, Tube Erosion Experience. *Material Issues in Circulating Fluidized Bed Combustors Workshop*, Argonne National Laboratory, Argonne, Illinois, June 19-23.

Lyczkowski,R.W., Gidaspow,D., Solbrig,C.W., and Hughes,E.C.(1978). Characteristics and Stability Analysis of Transient One-dimensional Two-Phase Flow equations and their Finite Difference Approximations, *Nuclear Science and Engineering*, **66**, 378-396.

Prosperetti,A.,(1982). Numerical Aspects of the Simmer-II Code. in *Multiple Process in LMFBR Safety Analysis*. Ispra, Italy, April, 197-224.

Rivard,W.C., and Torrey,M.D.(1977). K-FIX: A Computer Program for Transient, Two-Dimensional, Two-Fluid Flow, LA-NUREG-6623, Los Alamos.

Savage,S.B.(1988). Streaming Motions in a Bed of Vibrationally Fluidized Dry Granular Material. *J. Fluid Mech.*, **194**, 457-478.

Savage,S.B.(1983). Granular Flows at High Shear Rates. in *Theory of Dispersed Multiphase Flow* (ed. R.E.Meyer), Academic. 339-358

Soo,S.L.(1967). Fluid Dynamics of Multiphase System, Blaisdell Publ. Co., Waltham, MA.

Syamlal,M.(1985). Multiphase Hydrodynamics of Gas-Solids Flow. Ph.D. Thesis, Illinois Institute of Technology, Chicago.

Tsuo,Y.P., and Gidaspow,D.(1989). Computations of Flow Patterns in Circulating Fluidized Beds. presented at the *26th National Heat Transfer Conference*, Philadelphia, PA, August 9.

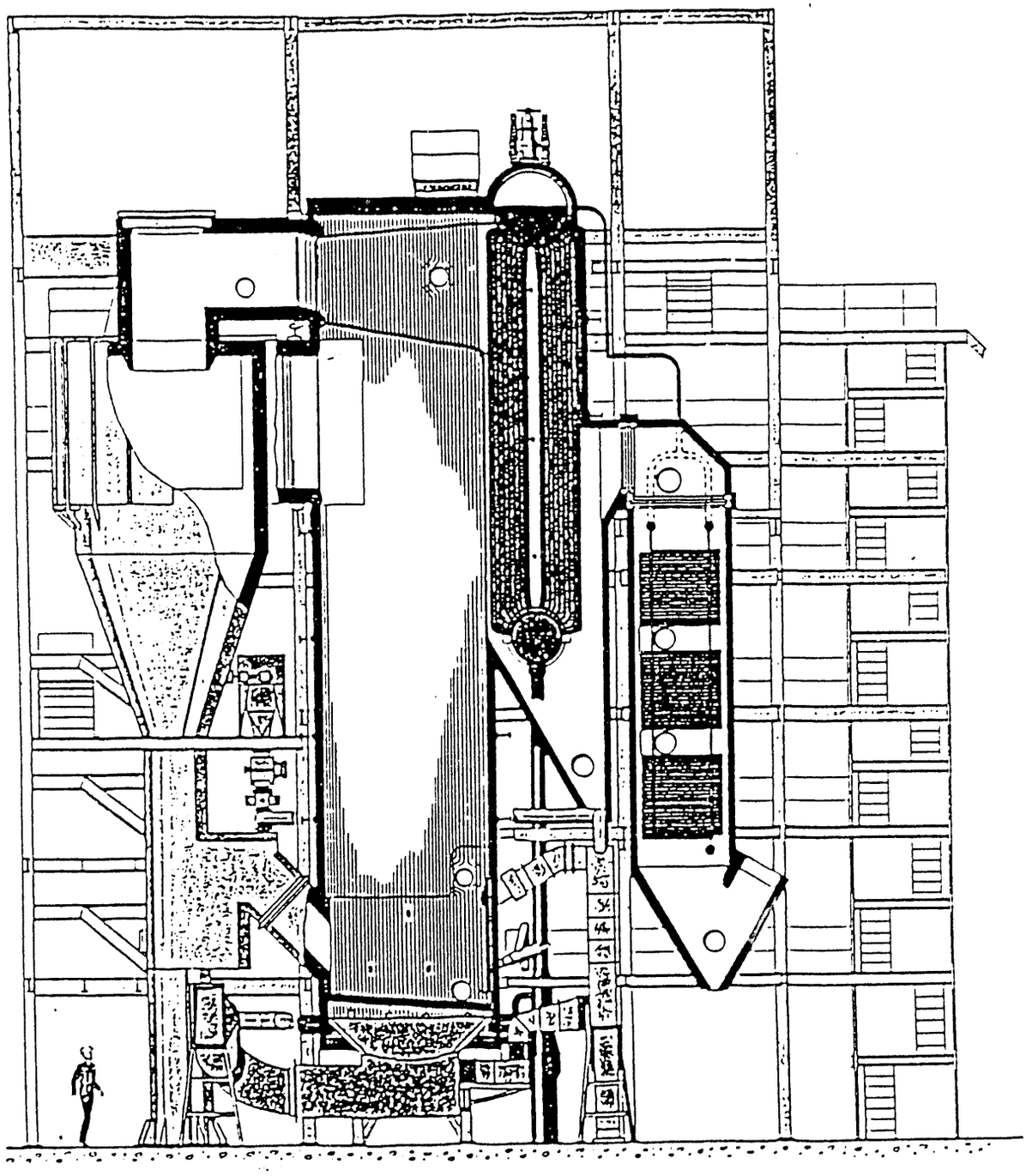

Figure 1. The PYROFLOW Circulating Fluidized Bed Combustion System

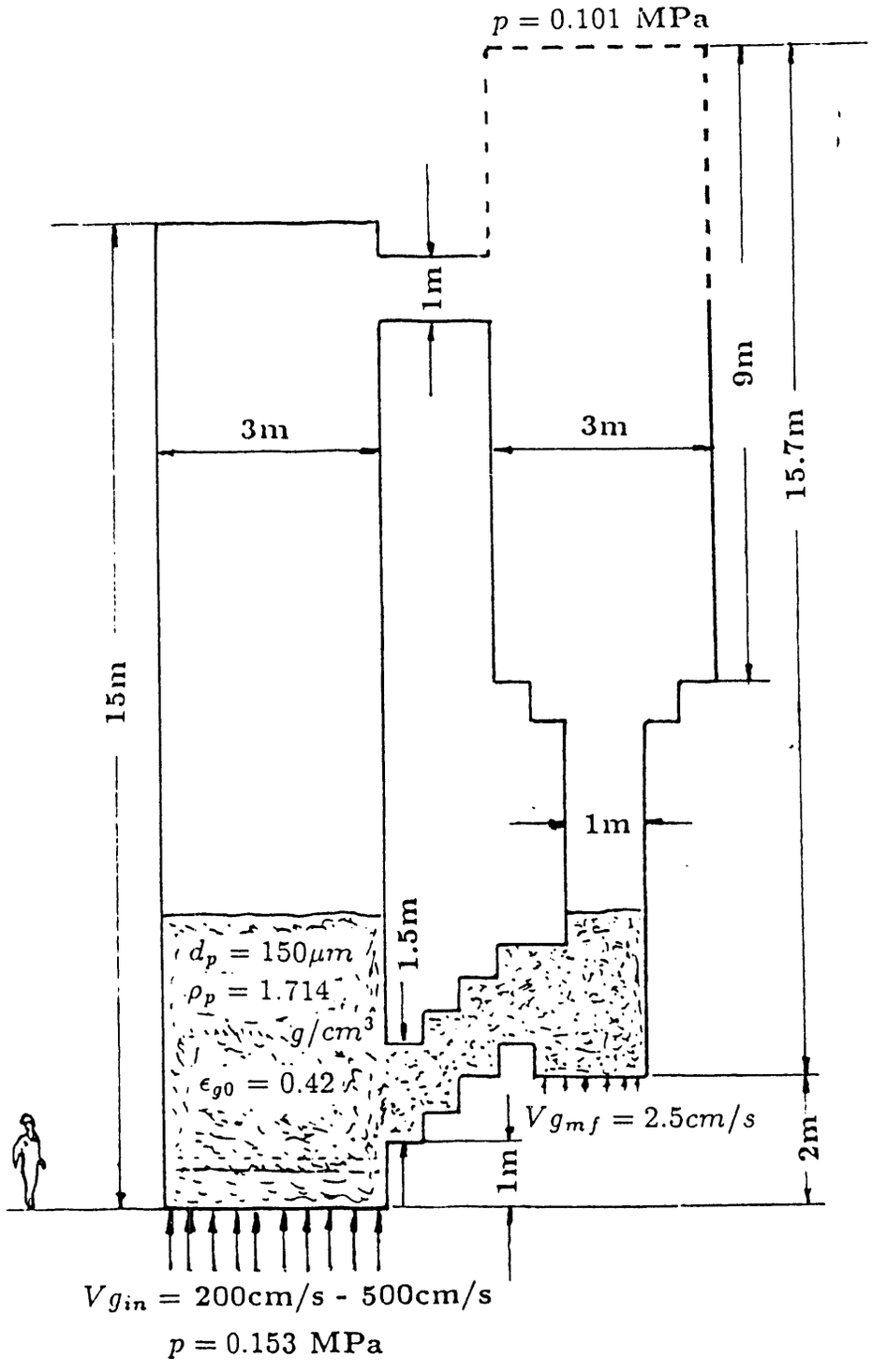

Figure 2. The Simplified Full-Scale PYROFLOW CFB with Dimensions and Flow Conditions

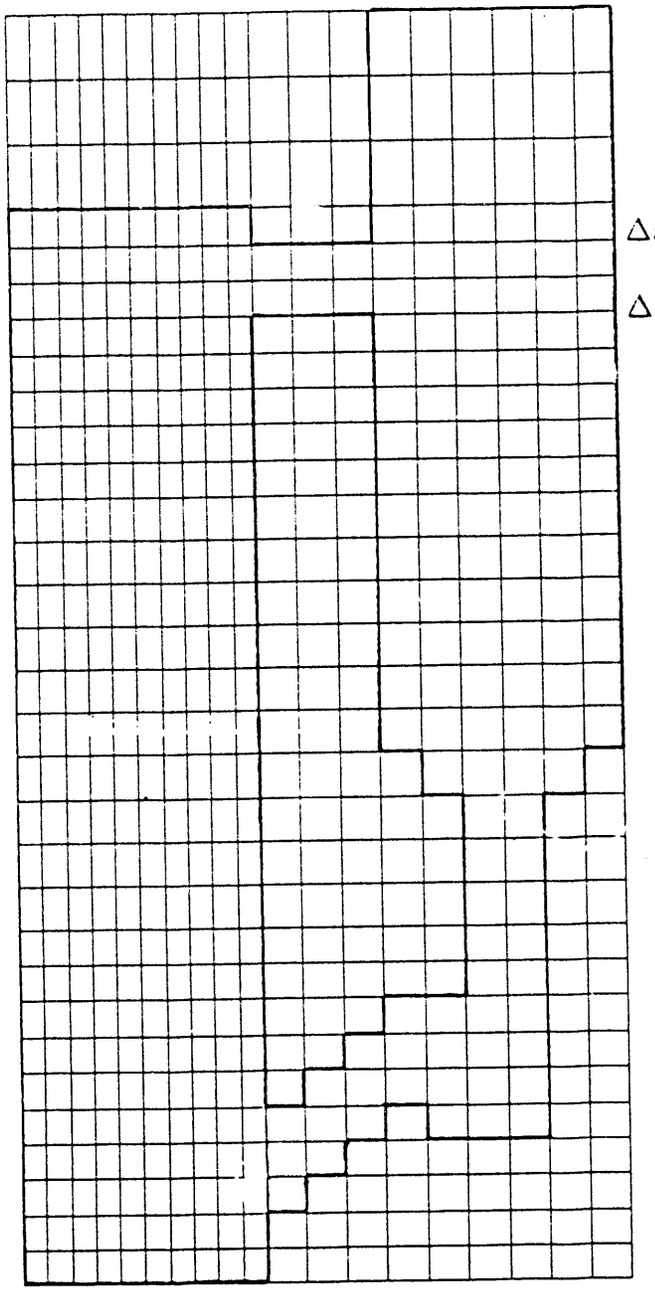

$\Delta x_{min} = 30cm \ \Delta x_{max} = 50cm$

$\Delta y_{min} = 50cm \ \Delta x_{max} = 90cm$

$\delta t = 0.0005 \ sec$

Figure 3. Non-Uniform Finite Difference Grids Used in the Computation

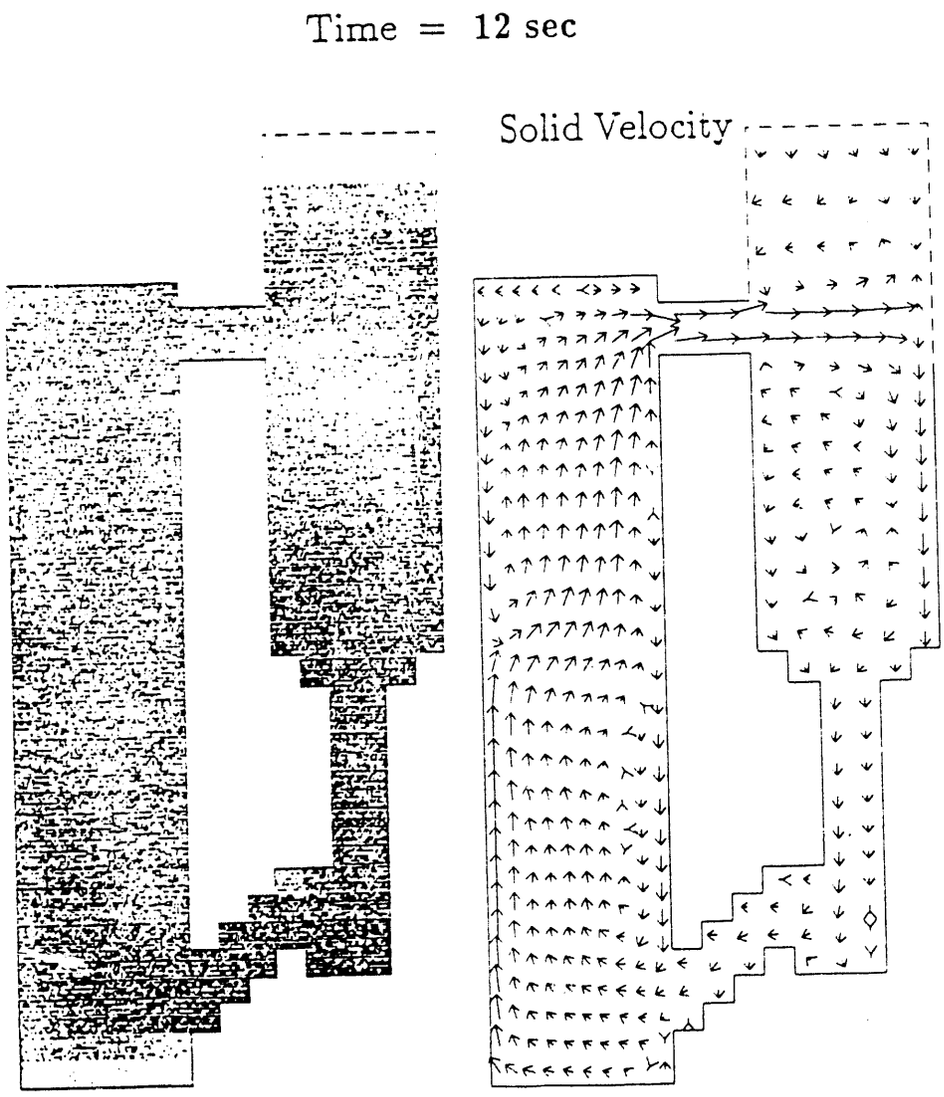

Figure 4. Particle Distribution and Solid Velocity at Time = 12 sec with $Vg_{in} = 200$ cm/s

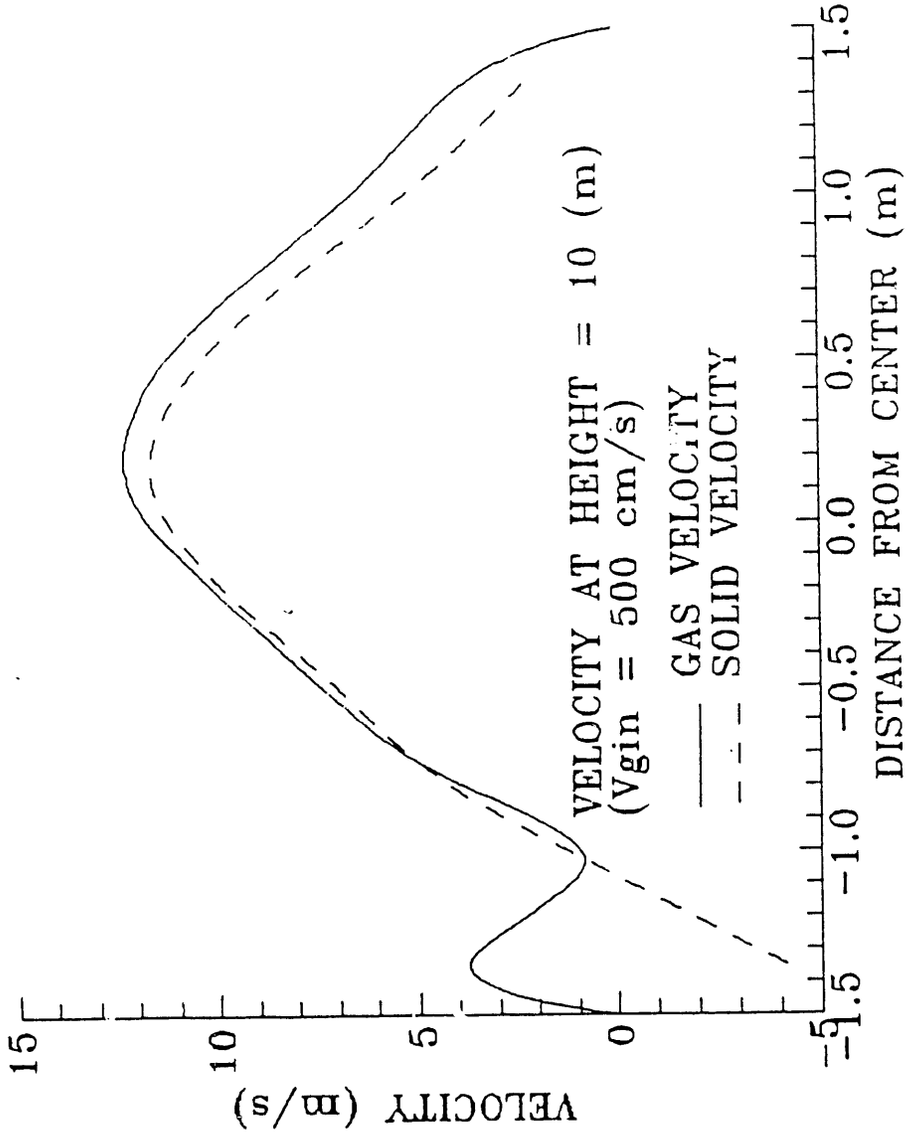

Figure 5. Radial Profiles of Axial Velocities at Height = 10 m with $Vg_{in} = 500$ cm/s

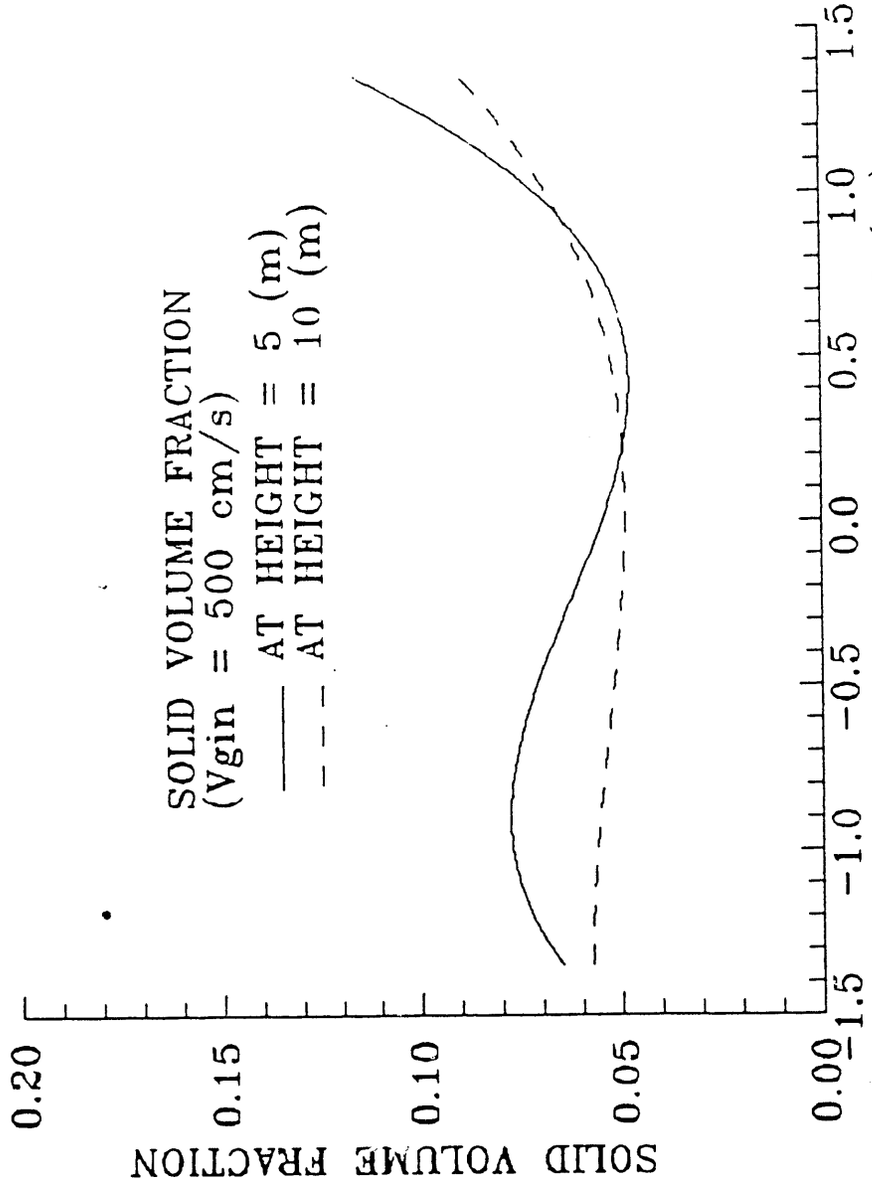

Figure 6. Radial Profiles of Solid Volume Fraction with $V_{g_{in}} = 500$ cm/s

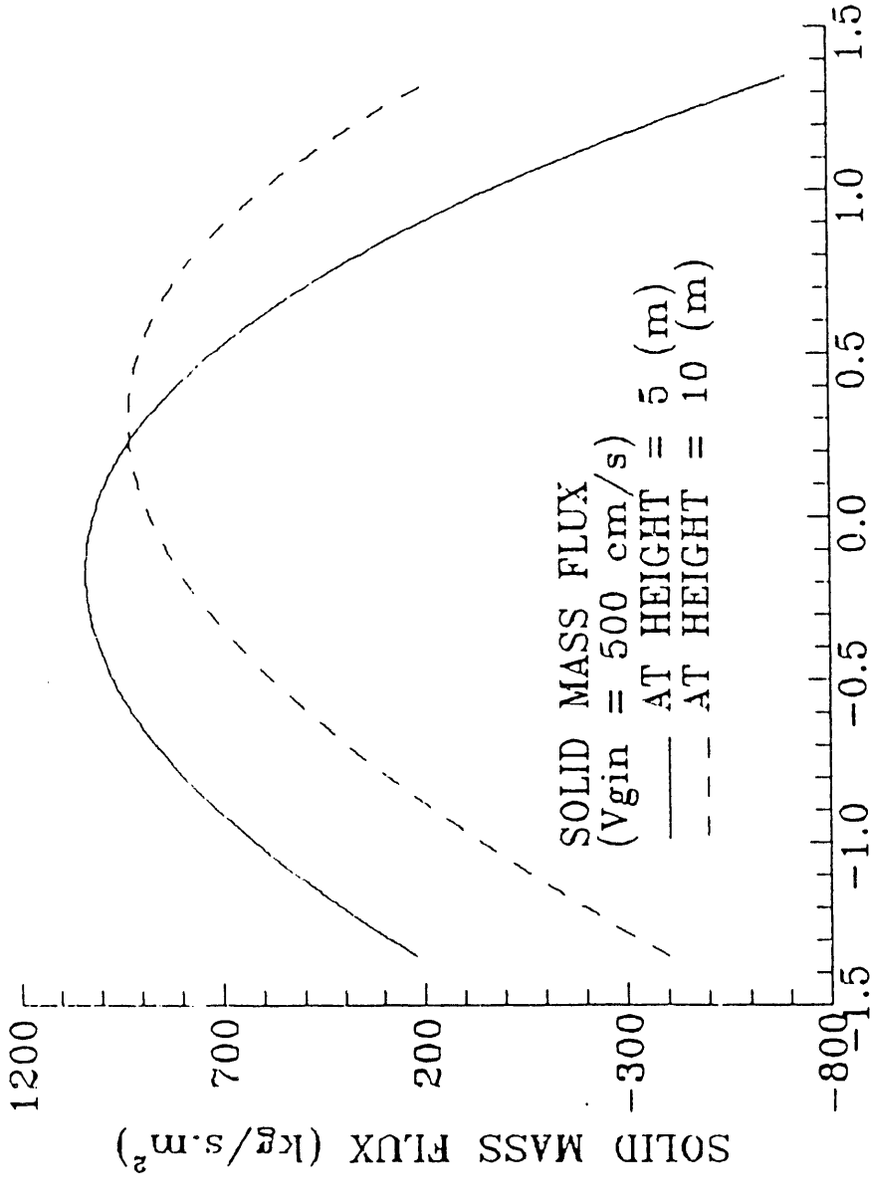

Figure 7. Radial Profiles of Solid Mass Flux with $Vg_{in} = 500$ cm/s

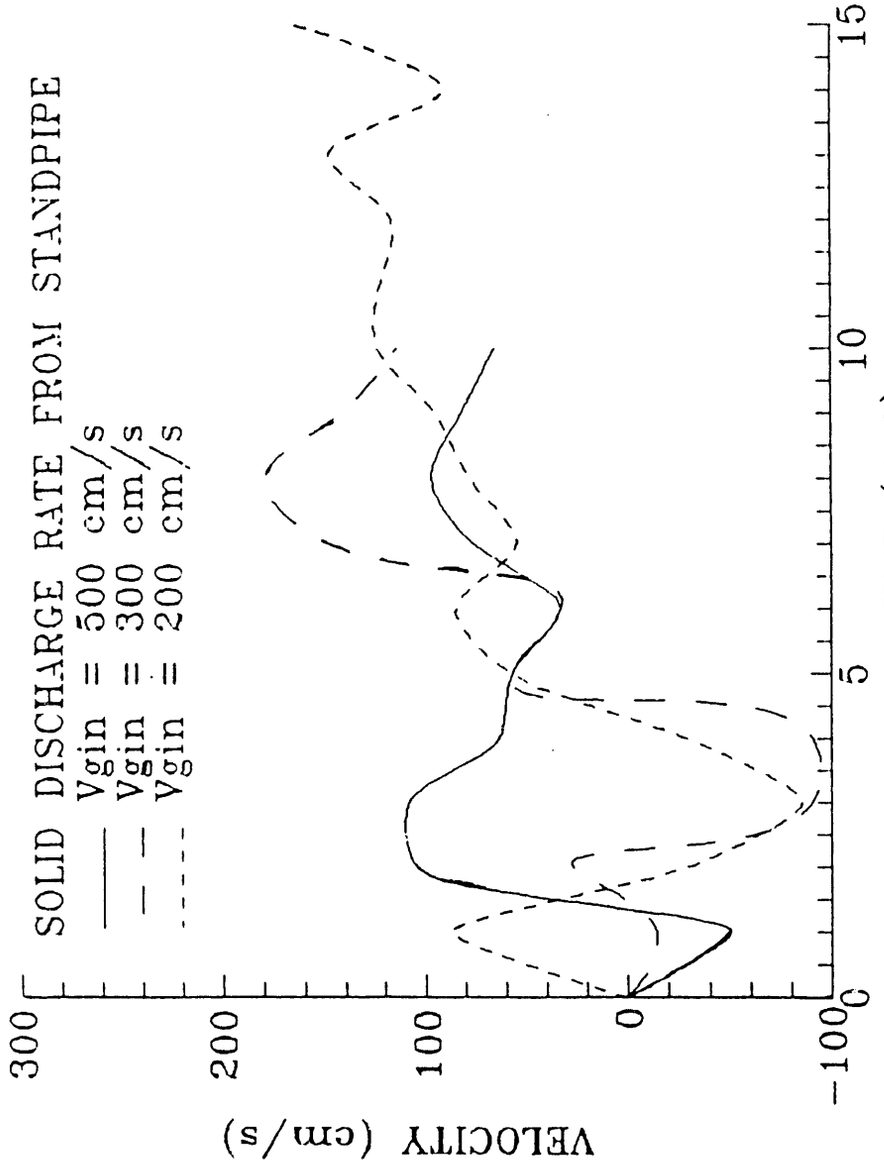

Figure 8. Solid Discharge Rate From the Standpipe to the Riser as a Function of Time

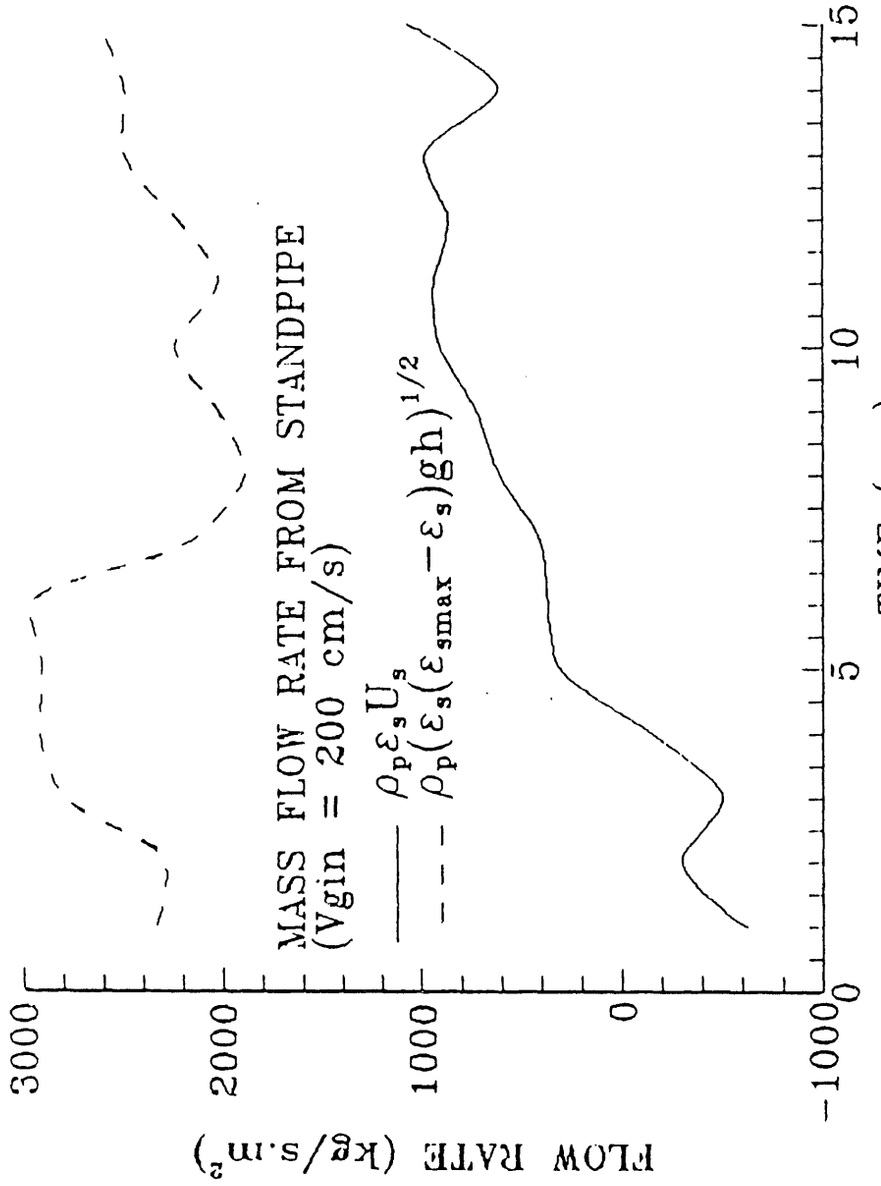

Figure 9. Inlet Solid Mass Flux versus Time (V_{gin} = 200 cm/s)

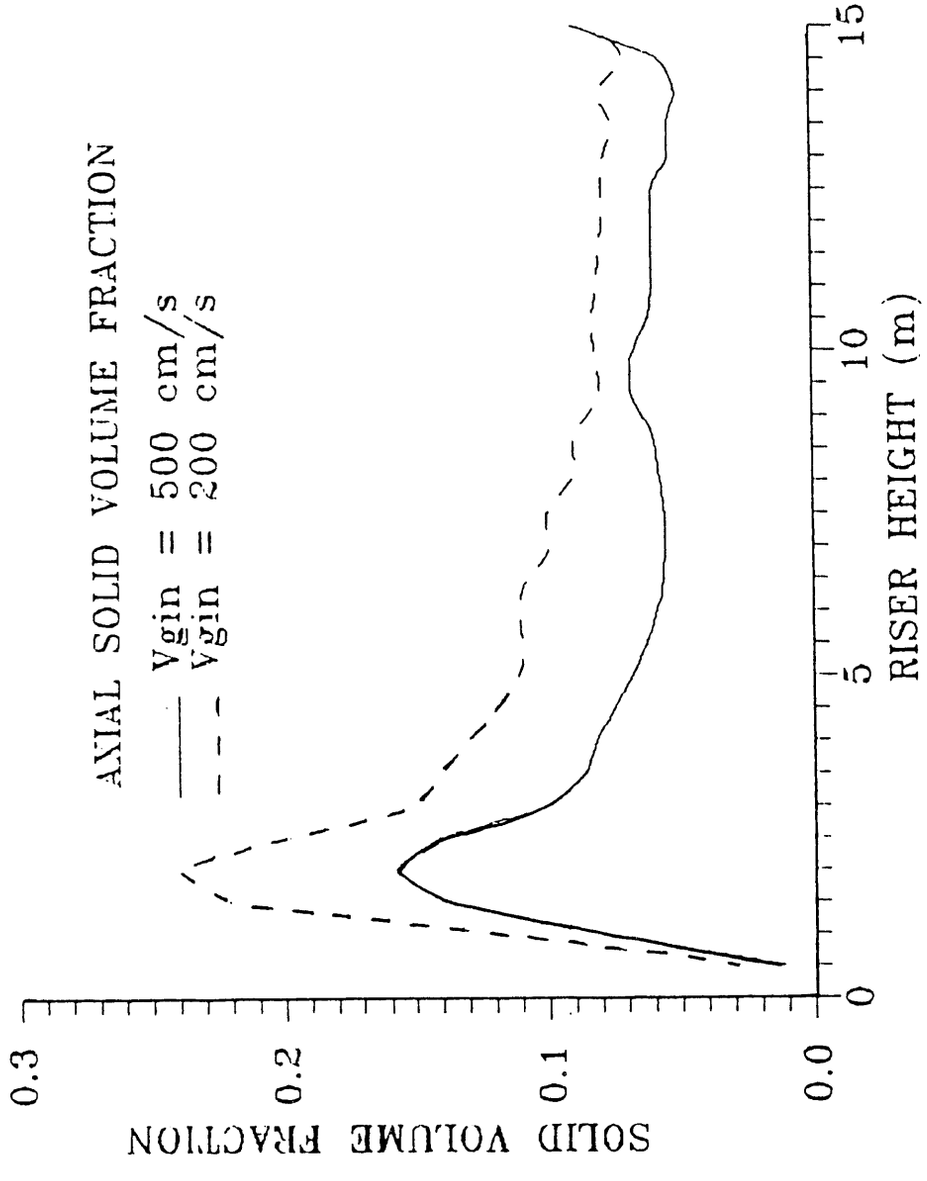

Figure 10. Area Averaged Solid Volume Fraction versus Riser Height

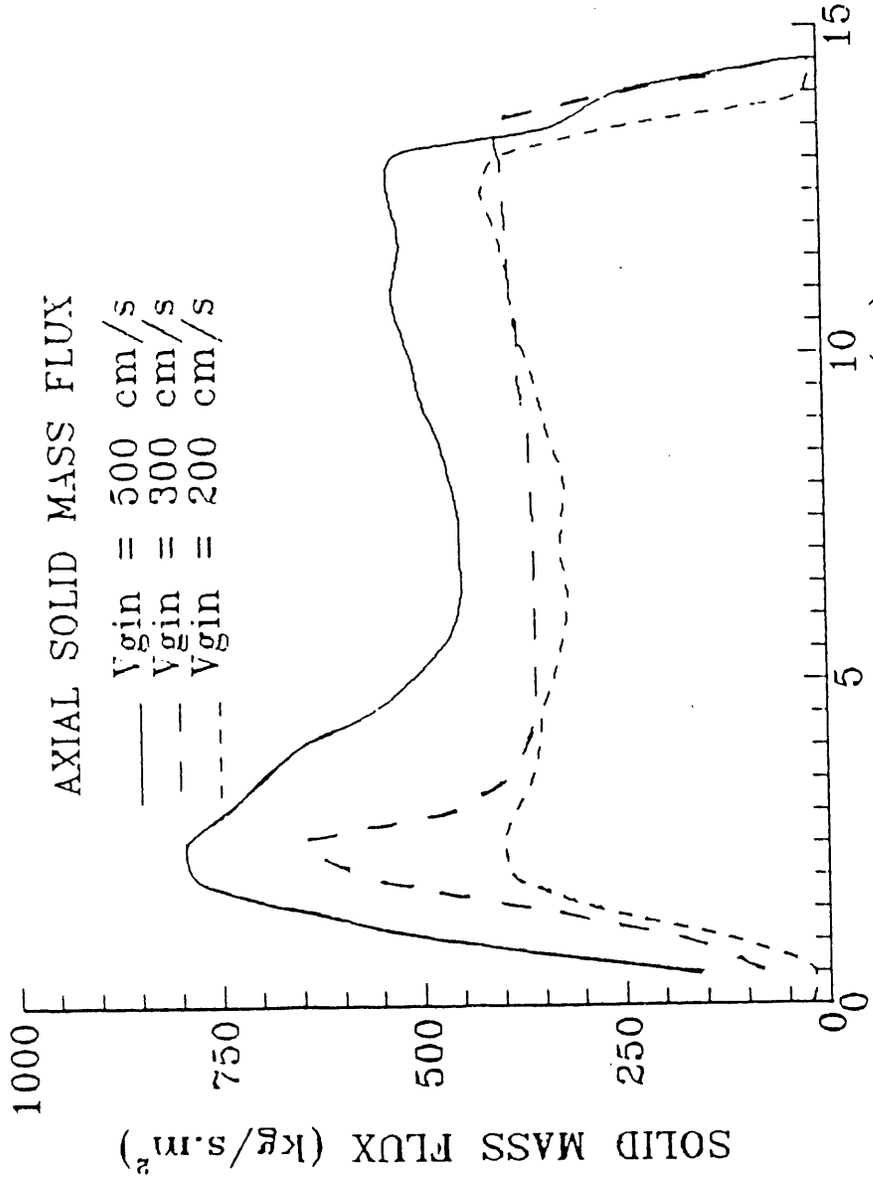

Figure 11. Area Averaged Solid Mass Flux versus Riser Height

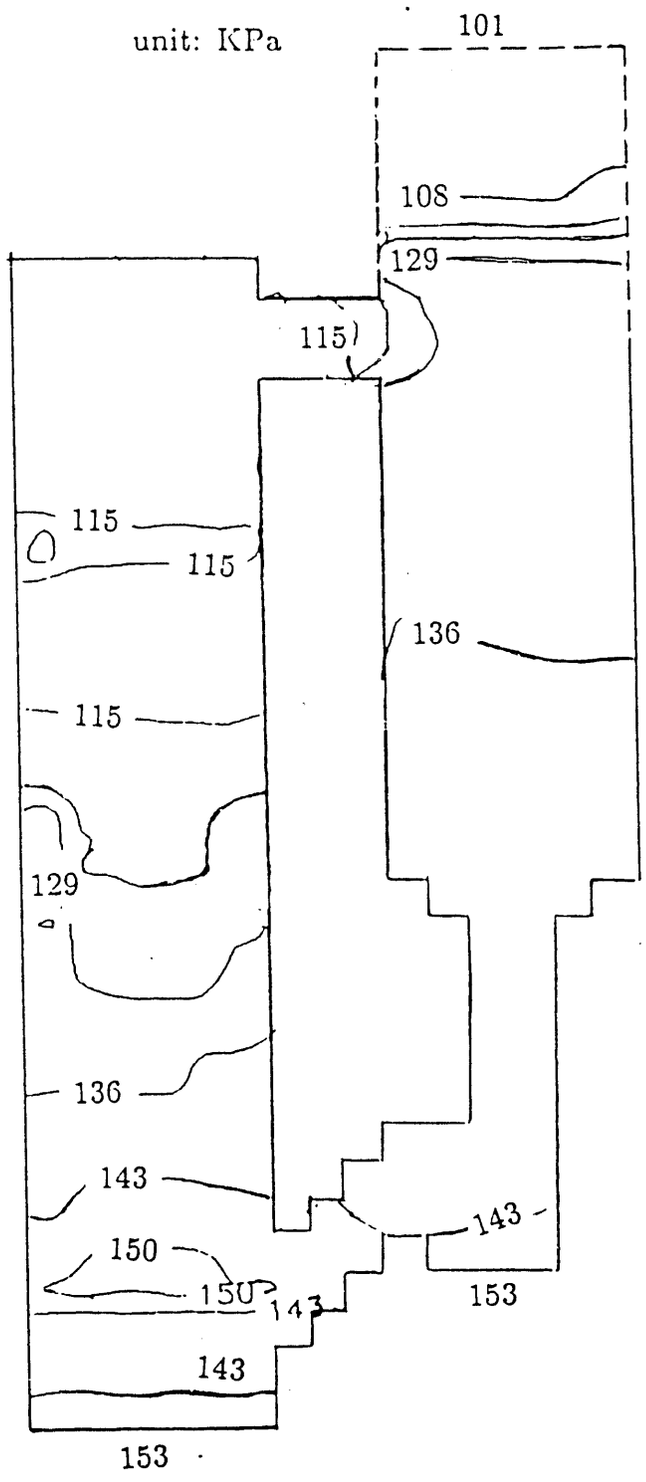

Figure 12. Time Averaged Pressure Distribution in the CFB with $Vgin = 500$ cm/s

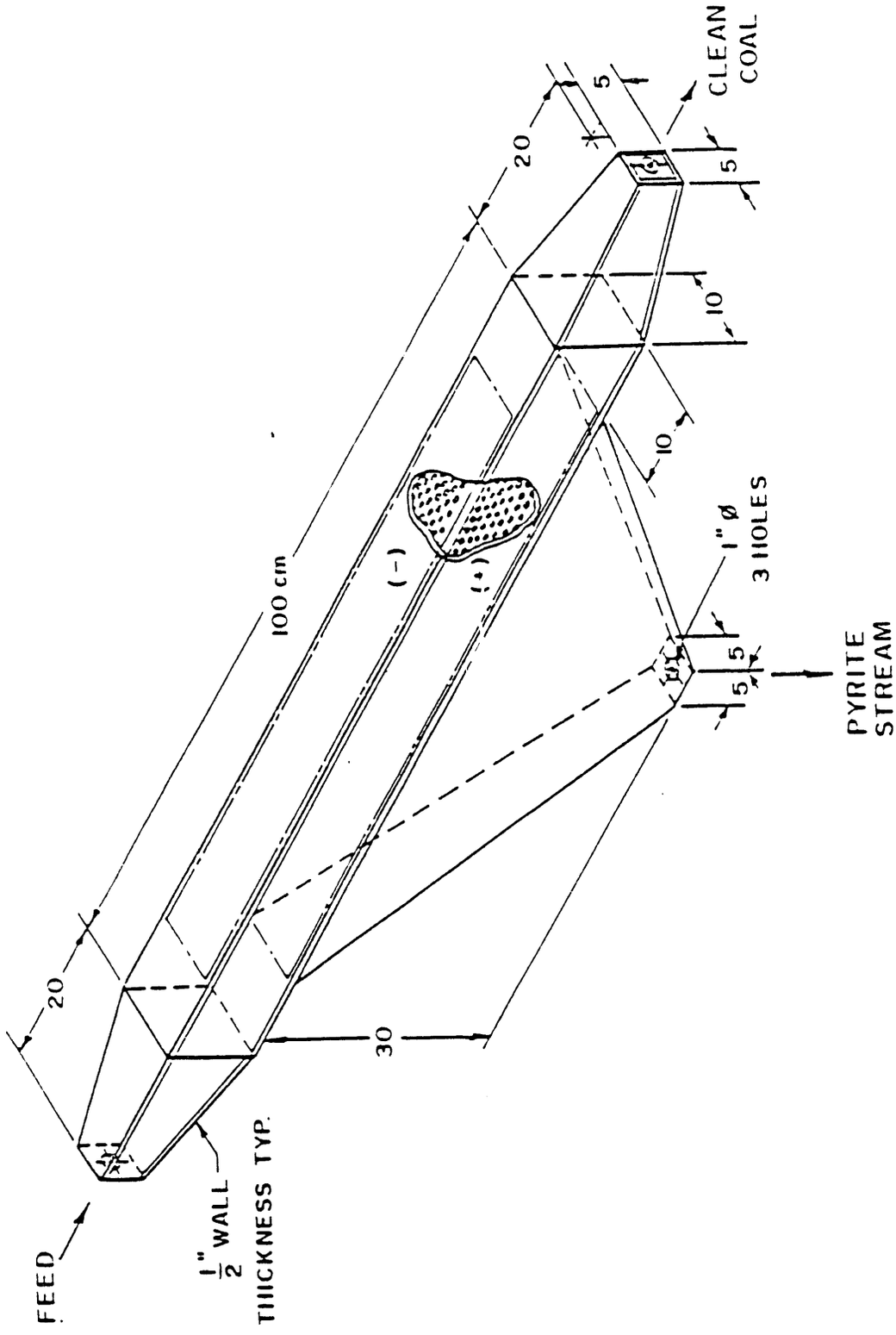

Figure 13. Electrostatic Sieve Conveyor.

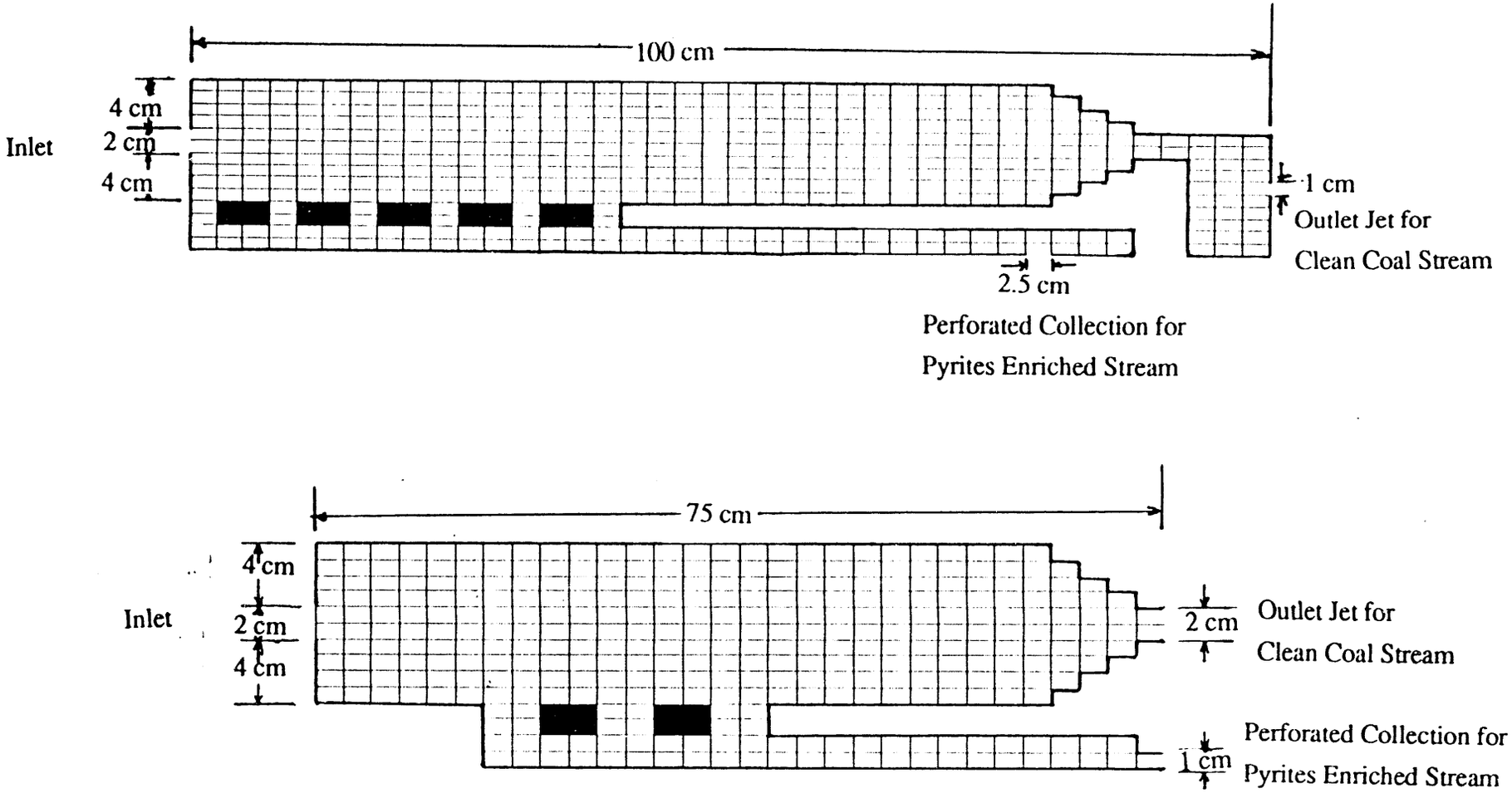

Figure 14.. Geometry of Electrostatic Separators (a) Unit I, and (b) Unit II (two dimensional cross-section is shown).

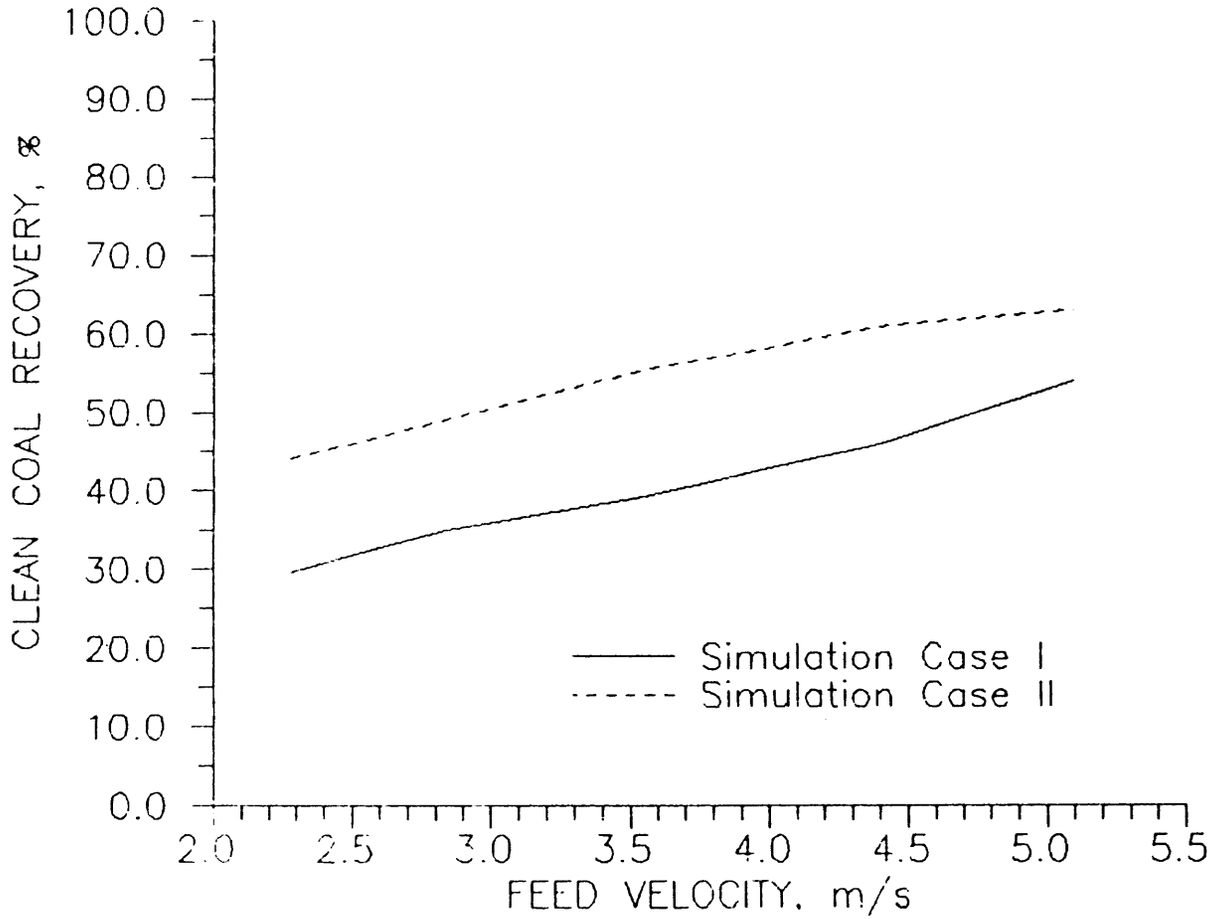

Figure 15. Clean Coal Recovery for Case I and Case II Simulations under same Operating Conditions.

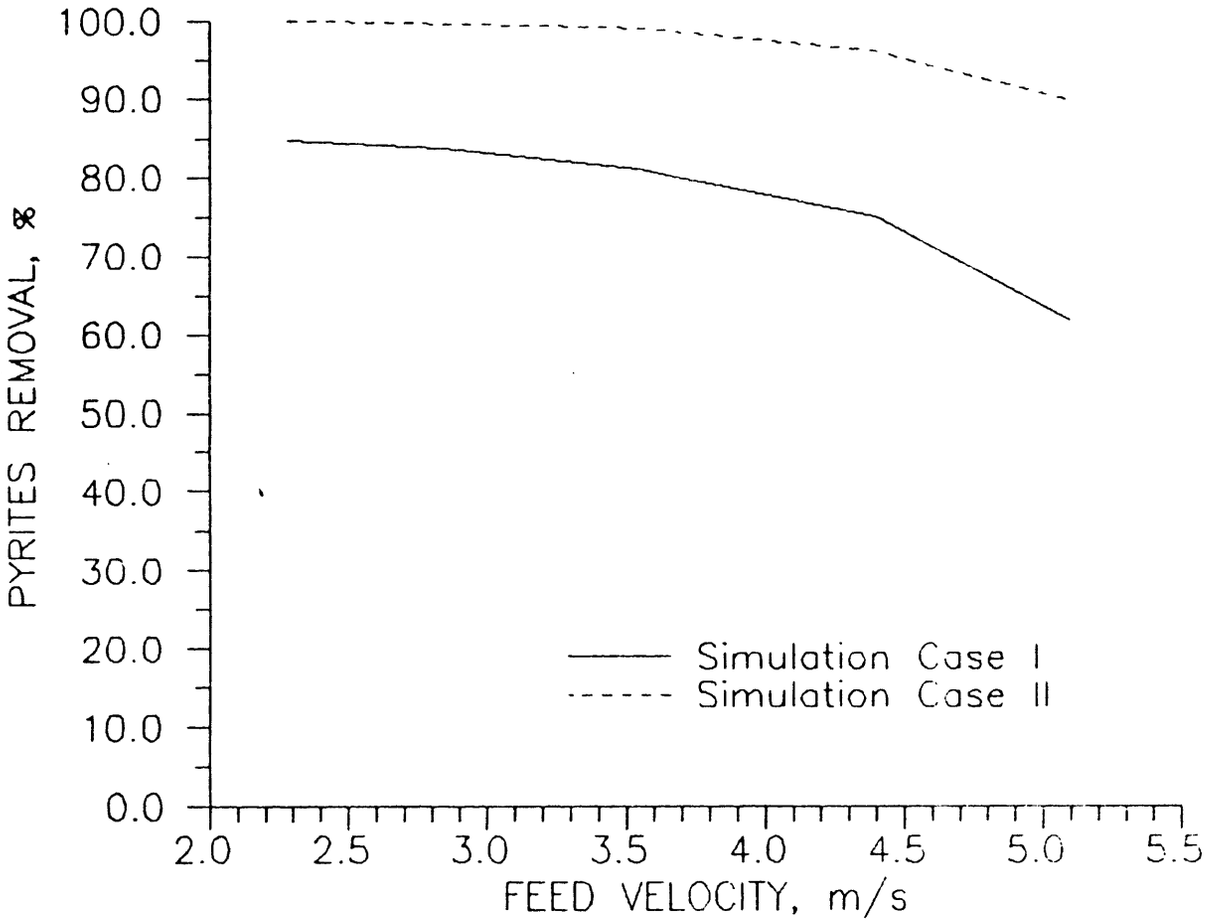

Figure 16. Pyrites Removal Case I and Case II Simulations under same Operating Conditions.

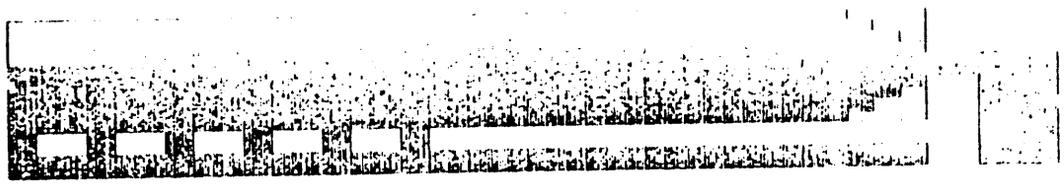

(a) Coal

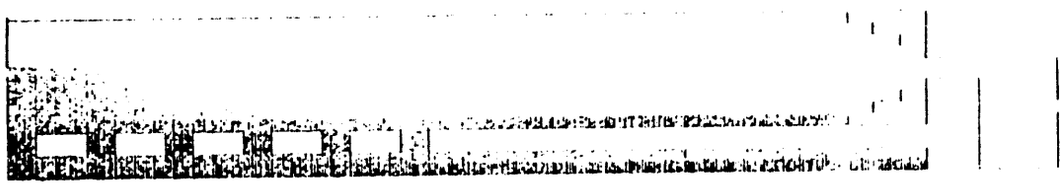

(b) Pyrites

Figure 17. Computed Concentration Density Plots in Electrostatic Separator at E = 1800 V/cm for Case I.

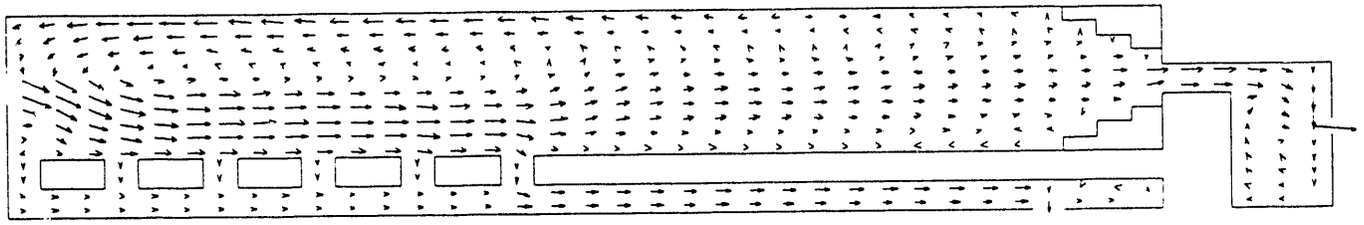

(a) Air

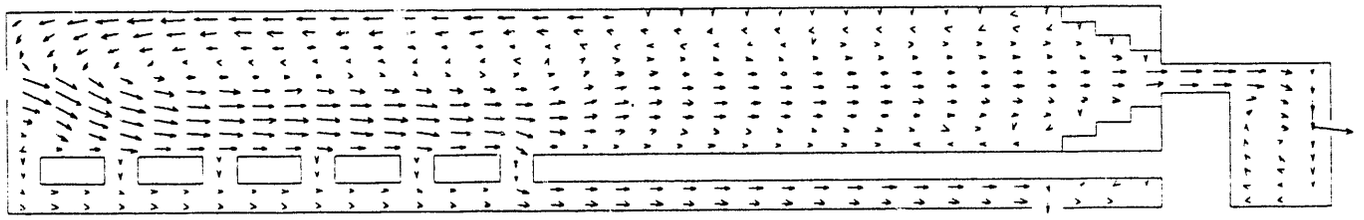

(b) Coal

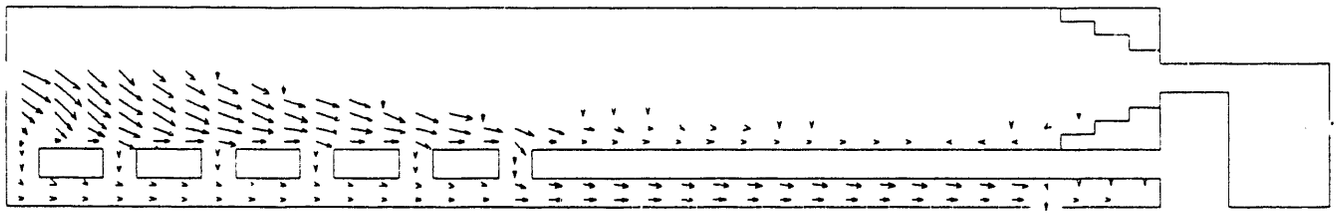

(c) Pyrites

Figure 18. Computed Velocity Profile Plots in Electrostatic Separator at E = 1800 V/cm for Case I.

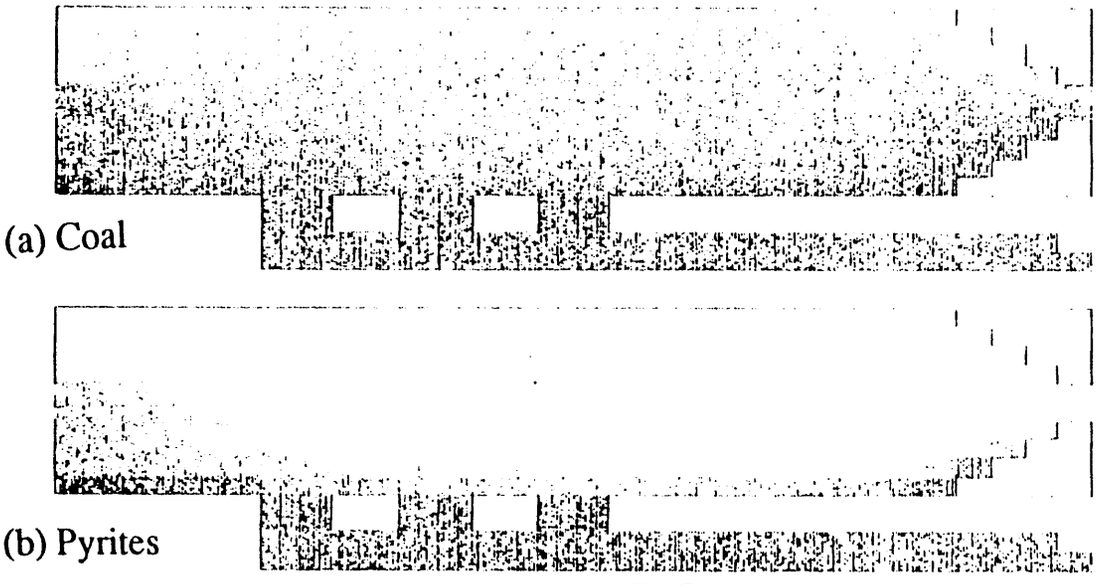

Figure 19. Computed Concentration Density Plots in Electrostatic Separator at E = 1800 V/cm for Case II.

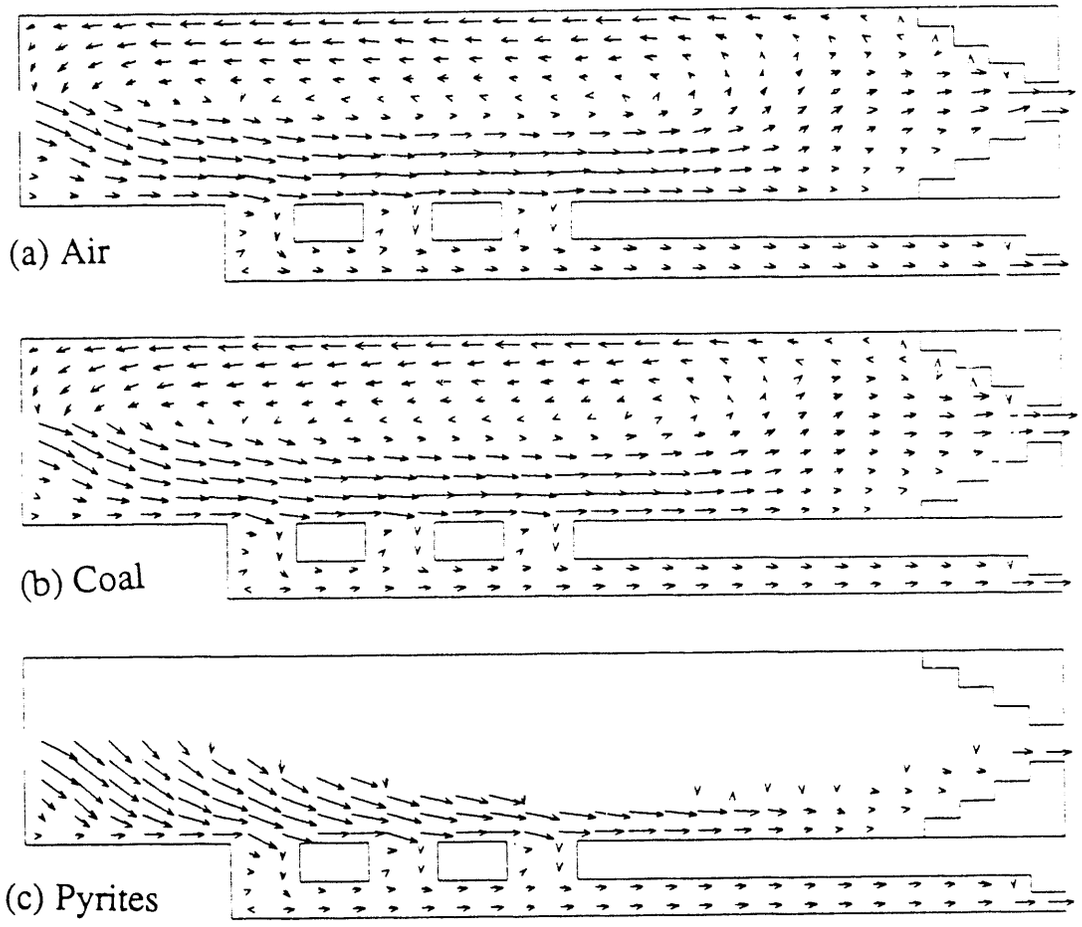

Figure 20. Computed Velocity Profile Plots in Electrostatic Separator at E = 1800 V/cm for Case II.

END

DATE FILMED

01/09/92